Conf-931108--97

UCRL-JC - 115773
PREPRINT

The Effects of In-Situ Processing Methods on The Microstructure and Fracture Toughness of $V-V_3Si$ Composites

M. J. Strum
G. A. Henshall
B. P. Bewlay
J. A. Sutliff
M. R. Jackson

This paper was prepared for submittal to
Materials Research Society 1993 Fall Meeting,
Boston, MA, November 29 - December 3, 1993

November 19, 1993

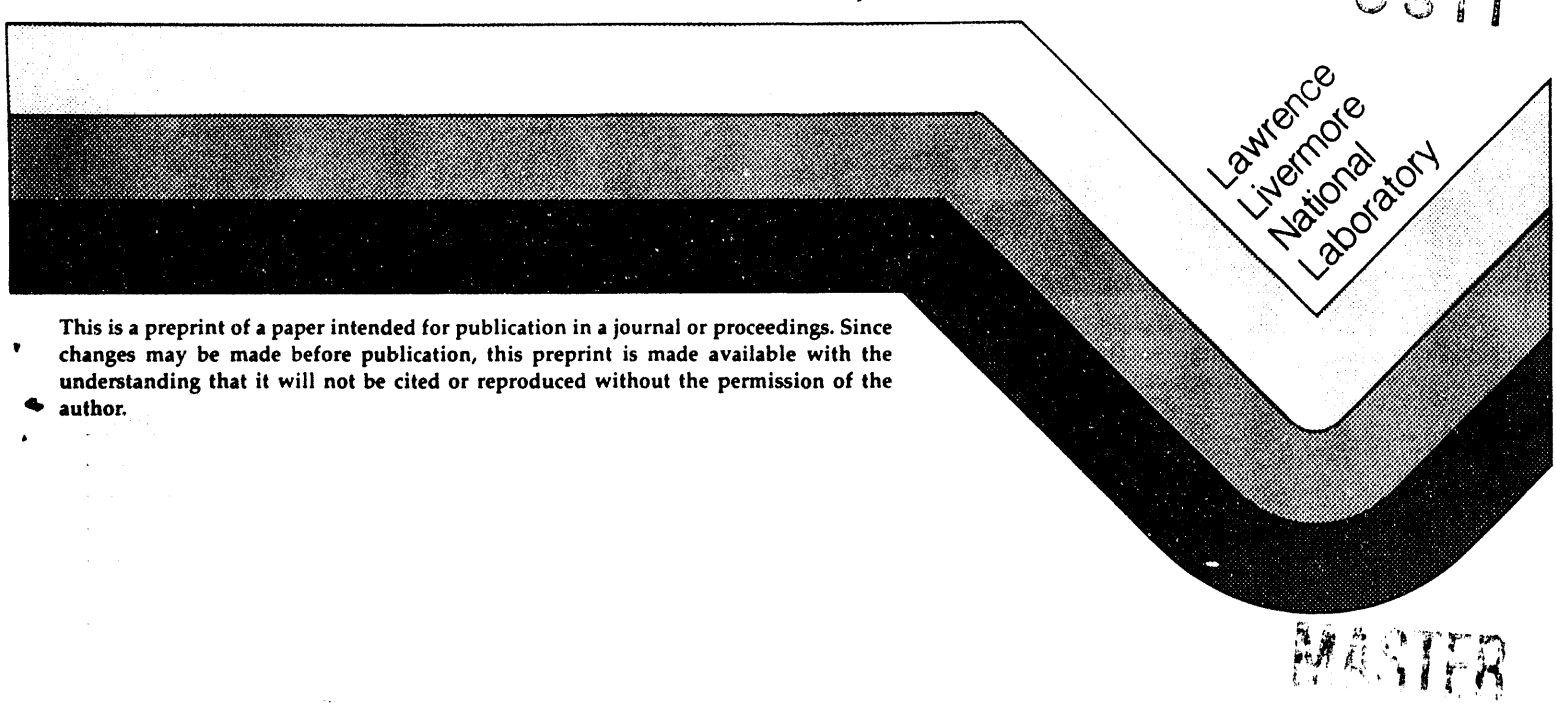

DISCLAIMER

THE EFFECTS OF IN-SITU PROCESSING METHODS ON THE MICROSTRUCTURE AND FRACTURE TOUGHNESS OF V-V_3Si COMPOSITES

M. J. Strum*, G. A. Henshall*, B. P. Bewlay**, J. A. Sutliff**, and M. R. Jackson**
*Lawrence Livermore National Laboratory, Livermore, CA 94550.
**GE Corporate Research and Development, Schenectady, NY 12301.

ABSTRACT

The present paper describes ductile-phase toughening in V-V_3Si in-situ composites that were produced by conventional arc melting (AM), cold-crucible induction melting (IM), and cold-crucible directional solidification (DS). Notched three-point bending tests were performed to determine the effects of synthesis method on the room temperature fracture toughness of eutectic compositions, which contain nearly equal volume fractions of V_3Si and the V(Si) solid solution phase. Fracture toughness values ranged from 10 MPa$\sqrt{m}$ for the AM eutectic to over 20 MPa$\sqrt{m}$ for the IM and DS eutectic alloys. SEM fractography, fracture surface profiling, and chemical analyses were performed to correlate the toughness values with the microstructures and interstitial concentrations produced by the three synthesis methods.

INTRODUCTION

Structural applications of refractory metal silicides and many other intermetallic compounds are limited by the low intrinsic fracture toughness of these materials in monolithic form. However, intermetallic ductile phase composites can possess substantially higher fracture toughness, as has been demonstrated using both artificial [1-4] and in-situ composite methods [5-7]. In-situ methods, in which a dispersed ductile phase is produced by phase separation during solidification, are especially attractive because they can minimize the cost of synthesizing the composite. However, the extent to which the microstructures can be tailored is more limited for in-situ composites than for artificial composites. Solidification conditions are a major variable through which in-situ composite microstructures can be optimized. In the present study, V-V_3Si eutectic composites were synthesized by: 1) conventional arc melting (AM), 2) cold-crucible induction melting (IM), and 3) cold-crucible directional solidification (DS). The influence of casting method and crack propagation direction on the room temperature fracture toughness were measured and compared.

The V-Si system contains a number of features desirable in a model system. The phase diagram contains a eutectic between the refractory metal intermetallic V_3Si and V(Si) solid solution at approximately 1870°C and contains no intermediate phases. The volume fraction of V_3Si in the eutectic is predicted to be 0.51 [8]. The V and V_3Si phases both have high melting points, 1910°C and 1925°C, and low densities, 6.0 g/cm^3 and 5.6 g/cm^3, respectively. The intermetallic V_3Si is an A15 compound, while V is among the most ductile of the refractory metals, with a ductile-to-brittle transition temperature below room temperature. Both the eutectic constituents exist as solid solutions within the castings, subsequently referred to as V_3Si and V(Si).

EXPERIMENTAL METHODS

Four eutectic V-V_3Si alloys were prepared using three casting methods. Eutectic alloy AM-1 was arc melted using pieces of high-purity V sheet, acid cleaned in HNO_3/HF solution, and vacuum degassed at 800°C for 1 h. The H concentration decreased substantially after the degassing treatment, with marginally detectable increases in N and O. The arc melted casting AM-2 and the IM and DS castings were prepared using V chips (120 ppm O, 80 ppm C, 26 ppm N, and < 3 ppm H) without acid cleaning. The silicon melting stock consisted of high-purity Si (99.999 wt.%) in all castings. The DS eutectic and IM eutectics were both produced in a segmented water-cooled copper crucible with a partially levitated melt [9]. Directional solidification was achieved using a Czochralski method in which a DS seed crystal was lowered

into the melt and withdrawn at 5 mm/min to produce a casting ~10 mm in diameter and ~100 mm in length. The IM casting was prepared similarly to the DS casting but was allowed to re-solidify within the crucible. All of the alloys were melted in high-purity argon atmospheres to minimize interstitial concentrations.

Chemical compositions for all of the castings were determined by spectrographic and LECO inert gas fusion methods and are listed in Table I. Interstitial concentrations were sensitive to both the V melting stock and the casting method. The degassed V sheet used in AM-1 produced a high O, N, and low H casting while the V chips in AM-2 produced a moderate O, N, and high H casting. The cold crucible techniques used for both the DS and IM castings produced relatively low O, N, and H concentrations.

Table I. Chemical compositions (by wt.)

Casting Method	Casting ID#	Si (%)	V (%)	O (ppm)	N (ppm)	H (ppm)
Arc Melt	AM-1	7.66	92.2	410	870	4
Arc Melt	AM-2	7.3	92.6	260	280	72
Directional Solidification	DS	7.3	92.6	130	58	22
Induction Melt	IM	7.25	92.7	200	30	9

Fracture toughness measurements were performed in three-point bending using single-edge-notched specimens with dimensions of approximately 3.5x7x30 mm. The specimens were tested at a span of 28 mm and a displacement rate of 0.02 mm/s. All specimens were fabricated and notched by electro-discharge machining (EDM) with a notch opening width of 0.3 mm and (a/w) of 0.45. Pre-cracking was performed under continuous loading and crack resistance data were measured by unloading immediately after each crack extension. Crack lengths were measured optically from metallographically polished specimen surfaces. The DS casting was tested in two orientations; with the direction of crack propagation either transverse or longitudinal to the DS direction. Because of the limited DS casting diameter, longitudinal DS specimens could not be machined directly into standard specimen dimensions. Instead, 8 mm sections of the casting were cut with the desired longitudinal crack orientation and brazed to two end pieces of eutectic material to produce specimens of the same dimensions as above. Brazing was performed in vacuum at a peak temperature of 965°C using a Ni-Au eutectic foil with a thickness of 0.05 mm. After brazing, the specimens were ground to final dimension and EDM notched.

Fracture profiles were prepared by electroplating 0.5 mm of Ni onto the fracture surfaces prior to sectioning and metallographic preparation. Backscattered electron imaging was used in the SEM, and phase interference contrast in the optical microscope, for improved contrast between the V(Si) and V_3Si phases.

RESULTS

The microstructures in each of the V-V_3Si castings consisted of eutectics between discontinuous V_3Si rods and a V(Si) matrix. The V_3Si volume fraction was measured for the DS casting as 0.48 using optical image analysis and the V(Si) and V_3Si compositions were measured as 4.5 and 20.1 at.% Si by electron probe microanalysis. Metallographic cross sections of the V_3Si rods revealed some degree of faceting, with equiaxed dimensions that varied in alignment and thickness along the rod lengths. Rod length-to-diameter ratios of up to 20:1 were present in all of the castings. In the AM and IM castings, the solidification structure was cellular, with cell diameters of 75 to 100 μm and lengths of 150 to 200 μm, as shown in Figure 1. The rod orientations were related within each cell core, but varied from cell to cell. The eutectic was coarser within the intercellular regions. The DS castings also possessed the cellular structure but the cells were highly elongated with cell diameters of 100 to 200 μm and lengths of at least 1.5 to 2 mm. The V_3Si rod lengths exhibited strong alignment with the DS growth direction within the cell cores, but the orientation varied within the intercellular regions, as shown in Figure 2. The rod diameters were larger in the DS casting than either the AM or IM castings. Typical rod diameters within the cell cores were between 1 and 1.5 μm in the AM and IM castings, and 1.5 to 3 μm in the DS casting. For all of the castings, the intercellular rods were up to 4 μm in diameter. The

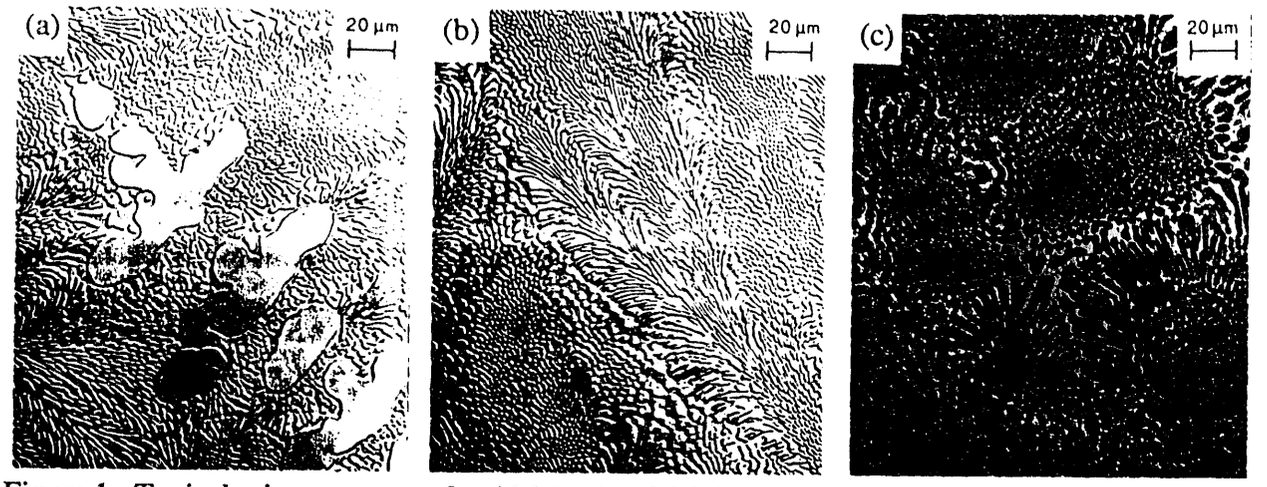

Figure 1. Typical microstructures for AM-1 (a). AM-2 (b), and IM (c) castings.

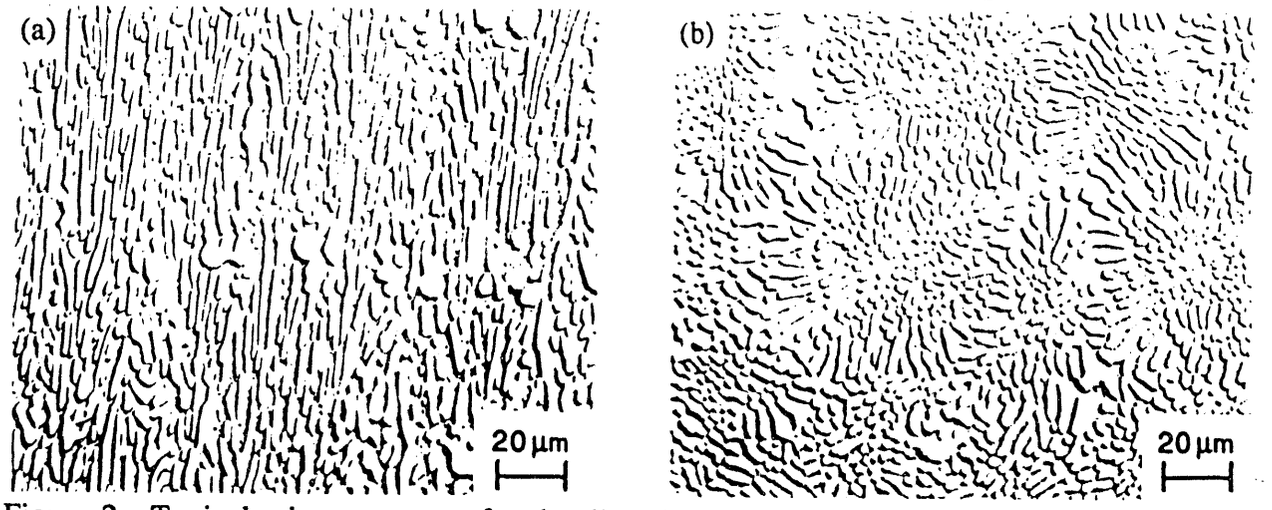

Figure 2. Typical microstructures for the directionally solidified casting in the longitudinal direction (a) and transverse direction (b).

V(Si) ligament dimensions increased with increasing rod diameter, as expected. In addition to the microstructural coarsening within the intercellular regions, occasional V_3Si dendrites were also present. These accounted for less than 1% of the casting volume except for the casting AM-1 (7.66Si), which contained approximately 2%. The AM-1 microstructure shown in Figure 1 represents the maximum amount of primary V_3Si observed.

As plotted in Figure 3, the toughness of castings AM-1 and AM-2 were similar, with average values of 10.4 and 10.6 MPa$\sqrt{m}$, respectively, . The toughness of the DS casting increased from an average of 14.4 MPa$\sqrt{m}$ for longitudinal crack propagation (DS-L) to 18.5 MPa$\sqrt{m}$ for crack propagation transverse to the crystal growth direction (DS-T). The highest average fracture toughness, 20.4 MPa$\sqrt{m}$, was measured in the IM casting. Fracture resistance data, plotted in Figure 3a, shows the absence of any significant changes in toughness with crack propagation. The data appear evenly scattered about the average values and indicate the absence of bridging zone development with increasing crack length.

The fracture surfaces of the AM, IM, and DS castings contained mixtures of large cleavage facets and fine micro-roughened zones, as shown in Figure 4. The size of the macroscopic cleavage facets and the cleavage area fraction were both highest in the AM castings, and decreased significantly for the DS and IM castings. Macroscopic cleavage zones typically consisted of a large number of facets corresponding to individual V_3Si rods connected by smooth or stepped regions corresponding to the intervening V(Si) ligaments. The extent of V(Si) stretching in these regions was minor, as shown in Figure 5 for the AM-2 casting. Conversely, the micro-roughened zones consisted of V_3Si rods containing secondary cracks and V(Si) ligaments which display considerable plastic extension. The bright contrast at the center of the stretched ligaments clearly

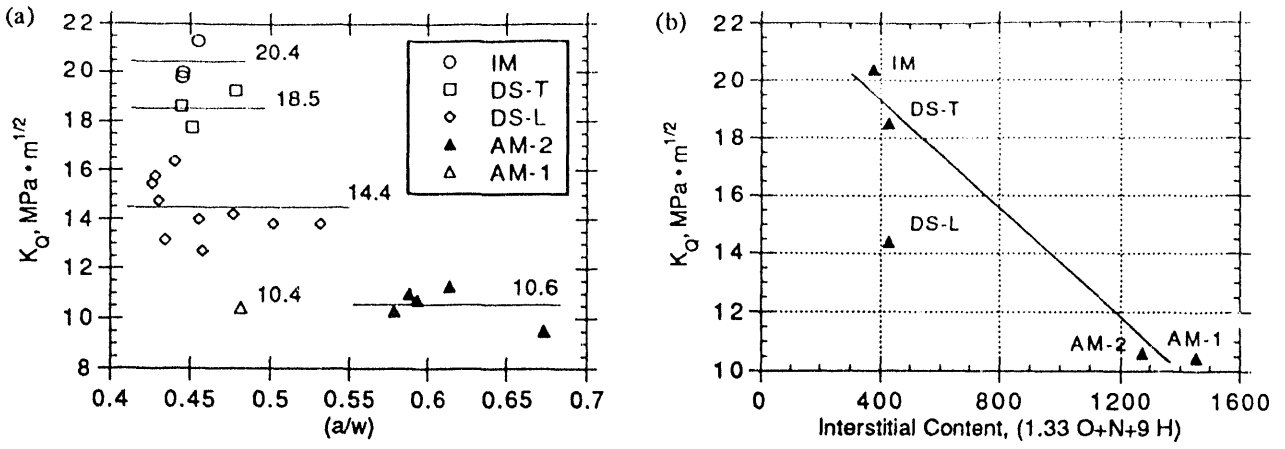

Figure 3. Fracture resistance data and average fracture toughness values for each casting (a), and fracture toughness vs. effective interstitial content (b).

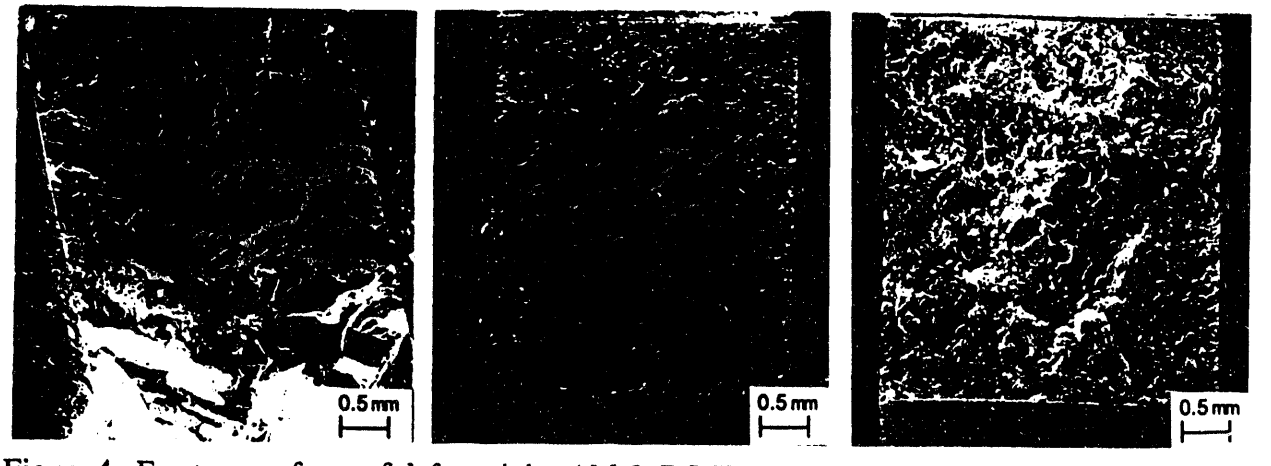

Figure 4. Fracture surfaces of, left to right, AM-2, DS-T, and IM castings.

outline each of the V_3Si rods. Similar features and contrast were observed in the IM casting.

Profiles of the fracture surfaces were prepared to quantify the magnitude of V(Si) plastic extensions beyond the V_3Si facets. However, unlike the apparently large plastic extensions viewed by SEM fractography, the presence of clearly visible V(Si) extensions was uncommon. The maximum plastic extensions measured were 0.33 to 0.66 μm for AM-2 , and 0.8 to 1.0 μm for the DS-T specimens.

DISCUSSION

The fracture toughness increased by a large increment for all of the eutectic composites relative to the toughness of monolithic V_3Si (< 1.3 MPa$\sqrt{m}$ [10]) with values from 10.4 to 20.4 MPa$\sqrt{m}$. Decreases in Si content from 7.66 (AM-1) to 7.3 wt.% (AM-2) reduced the quantity of primary V_3Si dendrites but had no significant effect on the fracture toughness, which only increased from 10.4 to 10.6 MPa$\sqrt{m}$. While the DS casting contained a coarser eutectic microstructure (indicative of the reduced thermal gradient and solidification rate during casting), the scale of the microstructure was similar for both the AM and IM castings, and therefore is unable to solely account for the toughness variations. The DS casting also contained a highly directional microstructure, with cells and rods strongly aligned in the growth direction within the cell cores.

The interstitial concentrations were affected by the synthesis methods, as shown in Table I, decreasing from the highest levels in the AM castings to much lower levels in the IM and DS castings. The influence of interstitial concentration on the Charpy impact toughness of pure V has been well documented [11], and the sensitivity to individual interstitial elements at room temperature was found to vary for N, O, and H in the ratio of 1 to 1.33 to 9, respectively. Assuming that this same ratio of interstitial sensitivities applies to the V(Si) ligaments, an effective

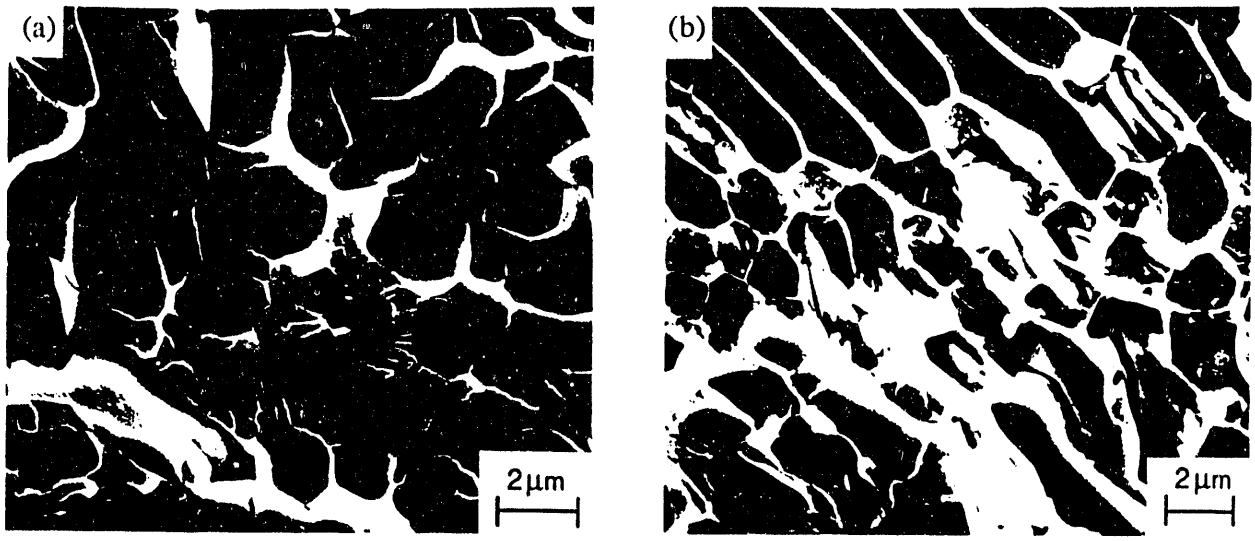

Figure 5. SEM fractographs of the cleavage region (a), and micro-roughened region (b) for AM-2.

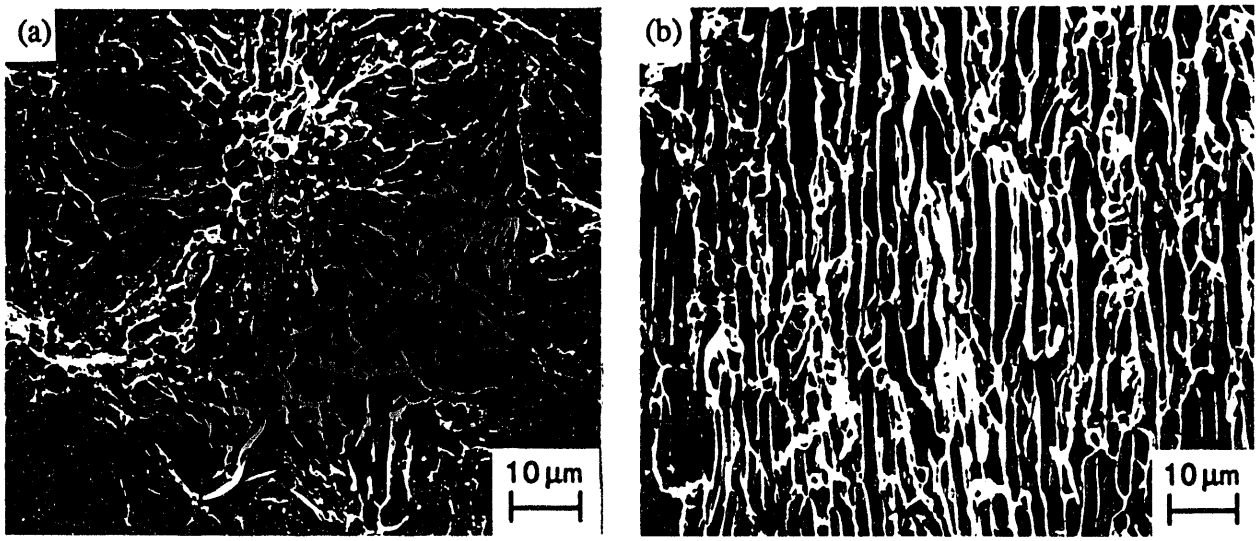

Figure 6. SEM fractographs of transverse (a) and longitudinal (b) crack growth orientations.

interstitial content was calculated for each casting and plotted vs. fracture toughness in Figure 3b. A linear fit to the data, for reference, reveals a good correlation for all of the test specimens with random or transverse rod orientations with respect to the crack propagation direction. Further increases in purity would be expected to provide additional toughening but the data are insufficient to predict a linear or exponential increase.

To determine the source of decreased toughness with longitudinal vs. transverse crack growth in the DS castings, one must consider the mechanism responsible for the eutectic toughening. The predominant toughening model used by others to describe both in-situ and artificial composite toughening by dispersion of a ductile phase is one of crack bridging [1,3,12-14]. In these models, the toughness should increase with increased ductile-phase stretching and with increasing crack length as the bridging zone is extended. In this study, the maximum ductile-phase extension measured is less than 1 μm, typically less than 0.33 μm, and only small bridging zones can be expected. The absence of toughness increases with crack propagation, shown in Figure 3a, is consistent with this behavior. Furthermore, the toughness dependence on the ductile phase fraction in AM V-V_3Si composites [10], suggests that a rule-of-mixtures model for the composite toughness may be more appropriate. In this case, the V(Si) phase largely determines the composite toughness due to the low toughness of the V_3Si. Increased composite toughness is expected from reduced interstitial concentrations which further increase the toughening contribution of the V(Si). The mechanism responsible for the decrease in toughness for crack propagation longitudinal (DS-

L) vs. transverse (DS-T) to the growth direction is under investigation, but may result from increased constraint in the V(Si) for the DS-L specimen. This behavior is predicted for cracks propagating parallel to the fiber (rod) direction [15] and would reduce the plastic energy dissipated during fracture.

CONCLUSIONS

The room temperature fracture toughness of V_3Si (< 1.3 MPa$\sqrt{m}$) can be increased by in-situ ductile-phase toughening with V. A toughness of over 20 MPa$\sqrt{m}$ has been measured for eutectic composites containing nearly equal volume fractions of V_3Si and V(Si) solid solution.

The toughness of V-V_3Si in-situ eutectic composites is sensitive to the method of synthesis. Measured toughness values range from 10 MPa$\sqrt{m}$ for AM material to over 20 MPa$\sqrt{m}$ for IM alloys. The sensitivity of fracture toughness to synthesis method is due to the resulting differences in interstitial impurity contents and the directionality of the microstructure with respect to the direction of crack propagation. A decrease in toughness was observed in DS material oriented with the direction of crack propagation parallel to the axis of the V_3Si rods, or growth direction.

Little ductile-phase extension was observed in fractured composites, and no increase in toughness with increasing crack length ("R-curve behavior") was observed. These results suggest that fracture toughness models based on crack bridging may be unsuccessful in simulating the behavior of V-V_3Si composites.

The fracture toughness decreases with increasing "effective" interstitial impurity content ([N]+1.33[O]+9[H]) for composites with a random or transverse orientation of the crack with respect to the axis of the V_3Si rods. Fracture toughness is predicted to increase above 20 MPa$\sqrt{m}$ for effective interstitial impurity concentrations below approximately 300 ppm.

ACKNOWLEDGMENTS

Work by two of the authors (MJS and GAH) was performed under the auspices of the U. S. DOE for the Lawrence Livermore National Laboratory under contract W-7405-Eng-48.

REFERENCES

1. L. S. Sigl, P. A. Mataga, B. J. Dalgleish, R. M. McMeeking, and A. G. Evans, Acta Metall. **36**, 945 (1988).
2. H. E. Deve, A. G. Evans, G. R. Odette, R. Mehrabian, M. L. Emiliani, and R. J. Hecht, Acta Metall. **38**, 1491 (1990).
3. L. Xiao and R. Abbaschian, Met. Trans. 23A, 2863 (1992).
4. W. O. Soboyejo, K. T. Rao, S.M.L. Sastry, and R.O. Ritchie, Met. Trans **24A**, 585 (1993).
5. J.J. Lewandowski, D. Dimiduk, W. Kerr, and M. G. Mendiratta, in High Temperature/High Performance Composites, edited by F. D. Lemkey et. al. (Mater. Res. Soc. Symp. Proc. **120**, Reno, NV, 1988), pp 103-109.
6. D. L. Anton and D. M. Shah, in Intermetallic Matrix Composites, edited by D. L. Anton et. al. (Mater. Res. Soc. Symp. Proc. **194**, Pittsburg, PA, 1988), pp. 45-52.
7. M. G. Mendiratta, J. J. Lewandowski, and D. M. Dimiduk, Met. Trans. **22A**, 1573 (1991).
8. J. F. Smith, Bull. of Alloy Phase Diagrams **6**, 266 (1985).
9. K-M. Chang, B. P. Bewlay, J. A. Sutliff, and M. R. Jackson, J. of Metals 44, **59** (1992).
10. M. J. Strum, G. A. Henshall, in High Temperature Ordered Intermetallic Alloys V, edited by I. Baker et. al. (Mater. Res. Soc. Symp. Proc. **288**, Boston, MA), pp. 1093-1098.
11. B. A. Loomis and O. N. Carlson in Reactive Metals, edited by W. R. Clough (Interscience Publ, New York, 1958), p. 227.
12. M. F. Ashby, F. J. Blunt, and M. Bannister, Acta Metall. 37, 1847 (1989).
13. B. Budiansky, J. C. Amizago, and A. G. Evans, J. Mech. Phys. Solds 36, 167 (1988).
14. K. S. Ravichandran, Acta Metall. 40, 3349 (1989).
15. R. C. Wetherhold and L. K. Jain, Mater. Sci and Engr. A165, 91 (1993).

DATE
FILMED
5/2/94
END